Position-Insensitive Wireless Power Transfer Based on Nonlinear Resonant Circuits

Omar Abdelatty, Xiaoyu Wang, *Member, IEEE,* and Amir Mortazawi, *Fellow, IEEE*

***Abstract*— Near-field resonant-based wireless power transfer (WPT) technology has a significant impact in many applications ranging from charging of biomedical implants to electric vehicles. The design of robust WPT systems is challenging due to its position-dependent power transfer efficiency (PTE). In this paper, a new approach is presented to address WPT's strong sensitivity to the coupling factor variation between the transmit and receive coils. The introduced technique relies on harnessing the unique properties of a specific class of nonlinear resonant circuits to design position-insensitive WPT systems that maintain a high PTE [1]over large transmission distances and misalignments without tuning the source's operating frequency or employing tunable matching networks, as well as any active feedback/control circuitry. A nonlinear-resonant-based WPT circuit capable of transmitting 60 W at 2.25 MHz is designed and fabricated. The circuit maintains a high PTE of 86% over a transmission distance variation of 20 cm. Furthermore, transmit power and PTE are maintained over a large lateral misalignment up to ±50% of the coil diameter, and angular misalignment up to ±75°. The new design approach enhances the performance of WPT systems by significantly extending the range of coupling factors over which both load power and high PTE are maintained.**

***Index Terms*— Frequency splitting, near-field wireless power transfer, power transfer efficiency, position-insensitive, passive nonlinear resonators, and self-adaptive circuits.**

I. Introduction

NEAR-FIELD wireless power transfer (WPT) is an emerging technology that enables seamless, contactless electrical power transmission from microwatts to kilowatts power levels [1]–[3]. Near-field WPT technology utilizes time-varying electromagnetic (EM) fields to transfer energy between a charging pad (the transmitter) and a pick-up pad (the receiver) attached to an electronic device or a battery, either through magnetic field coupling (inductive WPT) [4]–[6] or electric field coupling (capacitive WPT) [7]–[9]. WPT technology has attracted much interest as it can deliver power conveniently without using power cords while maintaining the same performance as plug-in charging. Some applications that significantly benefit from wireless power transfer include the powering of biomedical implants, consumer electronics, robots, drones, and electric vehicles (EVs) [10]. Furthermore, WPT technology is expected to play an important role in the area of autonomous electric vehicles.

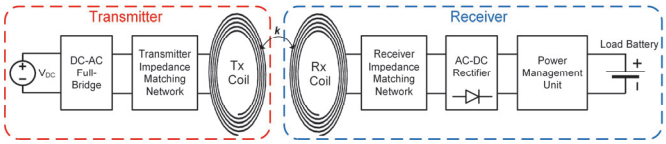

Fig. 1. Typical block diagram of an inductively coupled WPT system.

The block diagram of a typical magnetic resonance WPT system is shown in Fig. 1. In such a system, the power source drives the transmit coil, while the secondary coil in the receiver captures the transmitted magnetic fields. Subsequently, the received RF energy is converted to direct current (dc) via a rectifier and regulated using a power management unit before it is delivered to a load, often a rechargeable battery.

In order to achieve high power transfer efficiency (PTE) at considerable transmission range in an inductively coupled WPT system, resonance based WPT circuits have been proposed since non-resonant inductive WPT is highly inefficient [11]. In such circuits, resonators with high loaded quality factors (Q) are utilized. An important figure of merit in such systems, namely PTE which is defined as

$$PTE = P_L/P_{av,S} \quad (1)$$

where P_L is the power delivered to the load, and $P_{av,S}$ is the power available from the source. This definition for PTE considers both the source and the load matching, where $P_{av,S}$ is the maximum power that the source can provide under matched condition. Therefore, if the PTE is maintained as a function of the coupling factor, the output power delivered to the load also remains constant.

The strong dependence of the PTE in resonant-based WPT systems to the coupling factor between the transmit and receive coils is depicted in Fig. 2. The coupling factor is inversely proportional to the distance between the transmit and receive coils and the lateral/angular misalignment too [12]. At the optimum transmission distance, the transmit and receive coils

This paragraph of the first footnote will contain the date on which you submitted your paper for review. It will also contain support information, including sponsor and financial support acknowledgment. For example, "This work was supported in part by the U.S. Depart¬ment of Com¬merce under Grant BS123456."

The next few paragraphs should contain the authors' current affiliations, including current address and e-mail. For example, F. A. Author is with the National Institute of Standards and Technology, Boulder, CO 80305 USA (e-mail: author@ boulder.nist.gov).

S. B. Author, Jr., was with Rice University, Houston, TX 77005 USA. He is now with the Department of Physics, Colorado State University, Fort Collins, CO 80523 USA (e-mail: author@lamar.colostate.edu).

T. C. Author is with the Electrical Engineering Department, University of Colorado, Boulder, CO 80309 USA, on leave from the National Research Institute for Metals, Tsukuba, Japan (e-mail: author@nrim.go.jp).

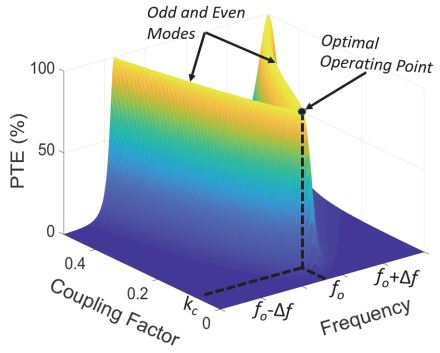

Fig. 2. PTE vs. operating frequency and coupling factor presenting the frequency splitting phenomenon for the conventional linear WPT systems.

are critically coupled and the load impedance is matched to the source impedance in order to satisfy the maximum power transfer condition. Hence, PTE is maximized when the resonant coils are critically coupled at the desired operating frequency. If the distance between the two coils is increased, the coupling factor decreases below the critical coupling value (the under-coupled region). In this region, the optimum frequency of operation remains the same, yet the PTE drops exponentially, as shown in Fig. 2. Conversely, at shorter distances, as the coupling factor increases above the critical coupling factor (the over-coupled region), a phenomenon known as frequency split occurs [13]. In this case, a high PTE can still be achieved but at two different frequencies away from the original operating frequency. Therefore, resonant-based inductively coupled WPT systems are prone to a significant PTE degradation as coupling factor varies.

In the real world, it is difficult to accurately control the distance and alignment between the transmitter and receiver in most WPT applications. For example, in electric vehicle charging, the driver has to park directly over the charging pad at an exact position due to the intolerance of WPT systems to misalignment. Although ground-viewing cameras and other parking assist systems have been proposed to help the driver to accurately park over the charging pad (e.g. the BMW 530e iPerformance wireless charging system, 2018), such systems are complex, costly, and not infallible. Moreover, different classes of EVs require customized charging pad design due to varying tire sizes and ground clearance. In dynamic charging scenarios, power is transferred to EV while driving over an array of transmitters, it is essential to maintain high PTE as the vehicle travels over the charging pads. Another example is the biomedical applications, where a high degree of reliability is important and the WPT performance must be maintained regardless of any misalignment between the transmit and receive coils. Additionally, in practical systems, the resonance frequencies of the resonators are affected due to environmental conditions, coupling to the nearby objects and component aging, hence degrading WPT power transmission efficiency. Therefore, practical WPT systems must be tolerant to coupling factor variation.

Several methods have been reported to improve the performance of near-field WPT systems [14]–[28]. It has been proposed in [16] to track one of the bifurcated modes (even and odd modes) in the over-coupled region by adjusting the source frequency in order to maintain high PTE. However, the frequency tracking range of this method is limited by the regulations of the Federal Communications Commission (FCC) regarding the allowable bands allocated for the WPT, mainly the Industrial, Scientific, and Medical (ISM) bands [17]. Therefore, this method cannot fully track the coupling factor variation within the entire over-coupled region. In addition, tunable matching circuits and switchable capacitor arrays [18]–[21] are proposed. However, the optimum impedance for maximum PTE varies drastically over distance, potentially making the impedance matching range unreasonable (high impedance matching range results in higher losses) and limiting the effective transmission distance [15]. Techniques of adjusting the coupling between multiple resonant loops [22]–[24], utilizing non-identical resonant coils [25], and using antiparallel resonant loops [26] are also introduced. Nevertheless, the extension of the transmission range provided by those techniques is limited due to the weak coupling factor. Thus-far, most of the approaches reported in the literature require sensing circuits and employ active feedback/control circuitry to adjust the circuit optimum operating point at each coupling factor. Therefore, these approaches are generally complex, increase systems' cost and size, and consume some overhead power for their operation. In [27], an alternative method is proposed where the RF power source is replaced by a parity–time symmetric circuit incorporating a nonlinear gain saturation element. However, the circuit's operating frequency varies as a function of the coupling factor, resembling the same drawback of the frequency tuning method. On the other hand, [28] proposes the combination between the electric and magnetic coupling to suppress the frequency splitting phenomenon. However, the variation in the power delivered to the load is significant and the structure of the proposed resonators is complex.

In this paper, a novel, self-adaptive nonlinear resonant based WPT circuits are introduced to maintain high PTE as the coupling factor varies within the over-coupled region by suppressing the frequency splitting phenomenon. The presented technique automatically adjusts the resonance frequencies of the coupled nonlinear resonators at each coupling factor between the transmit and receive coils without the need to adjust the source frequency, utilize active feedback/control circuits, or employ tunable impedance matching networks. The presented self-adaptive mechanism is accomplished by utilizing off-the-shelf passive nonlinear devices in the design of the WPT and energy harvesting circuits [29]–[33]. This work is distinguishable from [33] by presenting a general discussion of the duffing-type resonant circuits' properties, the working principle of the proposed position-insensitive WPT circuit, the nonlinear WPT circuit's modeling and analysis as well as the measurement setup and the experimental results of a 60 W WPT circuit prototype. The circuit employs a nonlinear resonant circuit at the receiver and exhibits a near-constant PTE of approximately 86% over a ±10 cm transmission distance variation from the desired transmission range.

The paper is organized as follows: the theoretical background and properties of the Duffing-type nonlinear resonant circuits are discussed in Section II. The principle of operation and analysis for the position-insensitive nonlinear resonant-based WPT circuits are described in Section III. The implementation and measurement results are presented in Section IV.

II. Theory and Properties of Electrical Nonlinear Resonant Circuits

The principle of operation for the position- insensitive WPT circuits relies on the behavior of a specific class of nonlinear resonant circuits known as Duffing resonators. In this section the unique characteristics of the forced harmonic oscillation of a nonlinear resonator described by a nonlinear differential equation referred to as Duffing Equation are discussed. The Duffing equation is used to characterize the mechanical resonances/oscillations with a nonlinear restoring force [34]. The basic form of the Duffing equation is given by,

$$\ddot{x} + 2\gamma\dot{x} + \omega_o^2\, x + \epsilon x^3 = Fcos(\omega t) \tag{2}$$

where x is the displacement, γ is the damping coefficient, ω_o is the oscillation frequency, ϵ is the third order nonlinearity coefficient, and $Fcos(\omega t)$ is the excitation force. The steady state solution of (2) can be approximated as $x(\omega, t) = X\, cos(\omega t - \theta)$, where X represents the amplitude, and θ represents the phase shift relative to the excitation signal [35]. The nonlinear resonators described by the Duffing equation demonstrate several important and unique properties that have been investigated in a number of fields including mathematics, physics, and mechanical engineering. The electrical representation of the Duffing-type nonlinear electrical resonator has been developed for the first time in [32] for wireless power harvesting applications to enhance the bandwidth of High-Q resonant circuits.

The basic schematic of a magnetically coupled nonlinear resonant-based WPT circuit described in this paper is shown in Fig. 3(a). The resonant circuit in the transmitter (primary circuit) is linear and driven by a sinusoidal voltage source $v_s(t) = V_s\, cos(\omega_s t)$, while the secondary resonator at the receiver side is nonlinear. In order to study the overall circuit behavior, an equivalent nonlinear RLC series resonant circuit with the same characteristics can be developed by referring the transmitter circuit to the receiver side as shown in Fig. 3(b). The basic series nonlinear electrical resonator is comprised of an inductor, a resistor, and a nonlinear capacitor, $C(v)$. The resonant circuit is driven by a sinusoidal voltage source $v_s\,(t) = V_s\ cos(\omega_s t)$. The C-V relationship of the nonlinear capacitor is symmetric (even function of voltage), i.e. $C(v_C) = C(-v_C)$, which can be either bell-shaped (Fig. 3(c)) or well-shaped (Fig. 3(d)). In general, a nonlinear inductor can also be used to provide the required nonlinearity. In this case, the nonlinear inductor's inductance must be an even function of the current.

The time domain dynamic equation describing the behavior of the nonlinear series RLC resonant circuit can be obtained by applying the Kirchhoff voltage law (KVL) and with the use of $i = dq\ /\ dt$:

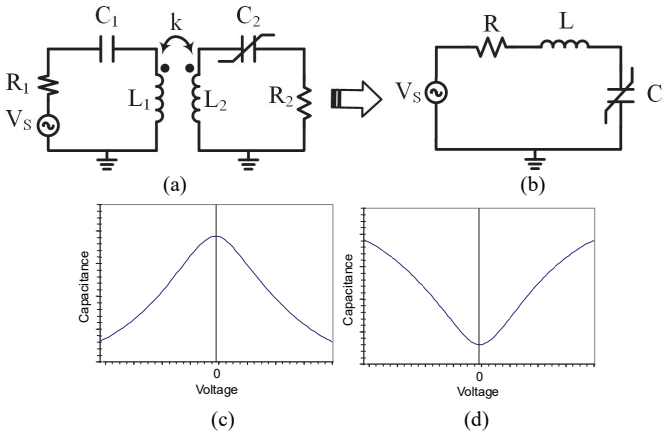

Fig. 3. (a) Nonlinear resonant-based inductively coupled WPT circuit, (b) equivalent single nonlinear series resonance circuit, (c) symmetrical bell-shaped C-V curve, and (d) symmetrical well-shaped C-V curve.

$$v_c(t) + R\frac{dq_c}{dt} + L\frac{d^2\, q_c}{dt^2} = v_s(t) \tag{3}$$

where $v_s(t) = V_S cos(\omega_S t)$ is the excitation voltage, $v_c(t)$ is the voltage across the nonlinear capacitor, and $q_c(t)$ is the amount of charge stored in the nonlinear capacitor. In order to express the voltage across the nonlinear capacitor in terms of charge q_c, the fundamental relationship between the voltage, current, and charge of the for a nonlinear capacitor is applied as follows,

$$dq_c = C\ dv_c + v_c\ dC \tag{4}$$

Thus, the total amount of stored charge during one cycle can be calculated by:

$$q_c = \int C\ dv_c + \int v_c\ dC = \int \left(C + v_c \frac{dC}{dv_c}\right) dv_c \tag{5}$$

The symmetric bell-shape C-V response of the nonlinear capacitor is approximately expressed by a polynomial of order n with even order terms assuming weak nonlinearity,

$$C = c_o + c_2 v_c^2 + c_4 v_c^4 + c_6 v_c^6 + \cdots + c_n v_c^n \tag{6}$$

The odd order coefficients can be negligible since the device is bilateral symmetric. This assumption was motivated by desire to express the differential equation governing the WPT circuit in the form of Duffing equation.

The voltage across the capacitor can be approximated with a truncated Taylor series, and by substituting (6) into (5), q_c can be written as:

$$q_c = \int \sum_{i=0}^{n(even)} (i+1) c_i v_c^i\ \ dv_c = \sum_{i=0}^{n(even)} c_i v_c^{i+1} \tag{7}$$

Since q_c is an odd function of v_c, the even order terms in the Taylor expansion of (7) vanish. Consequently, v_c can be expressed in terms of q_c, while neglecting terms higher than the third order for simplicity, using the inverse Taylor expansion,

$$v_c = \frac{1}{a_1} q_c + \frac{1}{a_3} q_c^3 \tag{8}$$

where $a_1 = c_o$ is the inverse of the linear coefficient and has a unit of C/V, and $a_3 = -c_o^4 c_2^{-1}$ is the inverse of the nonlinear

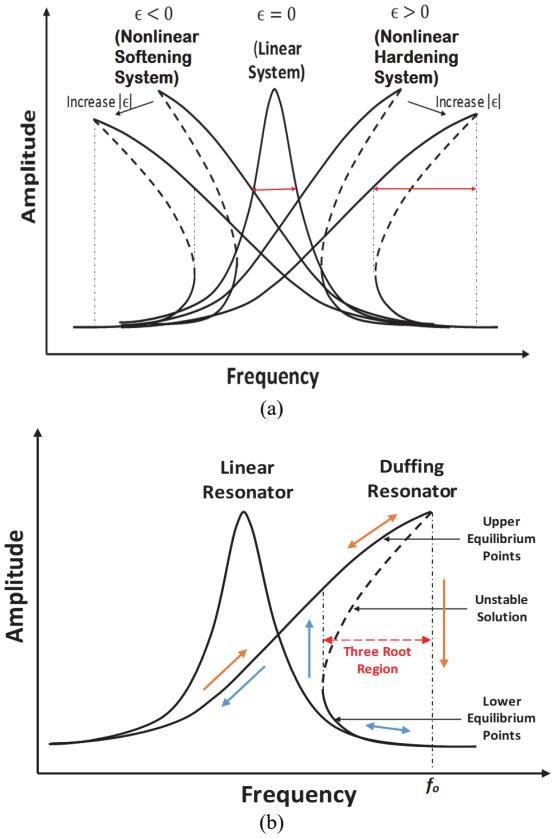

Fig. 4. The amplitude-frequency response of: (a) a single resonator with different nonlinearity coefficient (ϵ), (b) Duffing resonator (red and blue arrows show the hysteresis loop and jump phenomenon).

coefficient with a unit of C^3/V. In general, a_1 and a_3 can be calculated from the capacitance-voltage relationship for any nonlinear capacitor. Substituting (8) into (3) results in:

$$\ddot{q_c} + \frac{R}{L}\dot{q_c} + \frac{1}{La_1}q_c + \frac{1}{La_3}q_c^3 = \frac{V_s}{L}cos\,(\omega t) \qquad (9)$$

Equation (9) has the same form as the Duffing equation described in (2). The equation can be solved using the method of multiple scales, and the steady-state frequency response can be written as a sinusoidal function as follows:

$$q_c(t) = Q_c\,cos(\omega t - \theta) \qquad (10)$$

where Q_c represents the amplitude of the stored charge in the nonlinear capacitor, and θ represents the phase difference relative to the excitation signal. Both the linear term, $(1/La_1)q_c$, and the nonlinear term, $(1/La_3)q_c^3$, contribute to the restoring force. Therefore, an equivalent linear capacitance C_{eff} can be defined to quantify the restoring force contributed by the 3rd order nonlinear term,

$$\int_0^{T/2}\frac{1}{La_3}q_c^3\;dq_c = \int_0^{T/2}\frac{1}{LC_{eff}}q_c\,dq_c \qquad (11)$$

From (11), C_{eff} can be derived as:

$$c_{eff} = \frac{a_3}{\frac{3}{4}Q_c^2} \qquad (12)$$

Hence, the resonance frequency of the resonator, ω_o, in the presence of nonlinear restoring term can be written as:

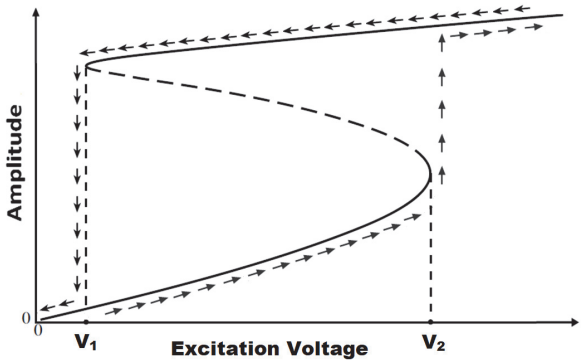

Fig. 5. The resonance amplitude versus excitation amplitude response.

$$\omega_o = \sqrt{\frac{1}{L}\left(\frac{1}{a_1} + \frac{1}{C_{eff}}\right)} = \sqrt{\frac{1}{L}\left(\frac{1}{a_1} + \frac{\frac{3}{4}Q_c^2}{a_3}\right)} \qquad (13)$$

Equation (13) implies that the resonance frequency, ω_o, depends on the nonlinear capacitor charge amount (Q_c), which is function of the voltage (v_c). The circuit's amplitude-frequency relationship of (9) can be expressed in the frequency domain as,

$$(j\omega)^2\mathcal{Q}_C + \frac{R}{L}(j\omega)\mathcal{Q}_C + \left(\frac{1}{La_1} + \frac{1}{LC_{eff}}\right)\mathcal{Q}_C = \frac{V_S}{L} \qquad (14)$$

where

$$\mathcal{Q}_C = Q_c e^{-j\theta} \qquad (15)$$

is the phasor form of $q_c(t)$. Substituting (12) and (15) into (14) yields,

$$Q_c^2\left(\frac{1}{La_1} + \frac{\frac{3}{4}Q_c^2}{La_3} - \omega^2\right)^2 + \left(\frac{R}{L}Q_c^2\omega\right)^2 = \left(\frac{V_S}{L}\right)^2 \qquad (16)$$

After determining the amplitude of Q_c, the magnitude of current flowing in the nonlinear resonator is determined by,

$$I = j\omega\mathcal{Q}_C \qquad (17)$$

Hence, the average power delivered to the resistive load can be calculated as follows,

$$P_{avg} = \frac{1}{2}|I|^2R \qquad (18)$$

Based on (16), the resonance amplitude (Q_c) as a function of the excitation frequency (frequency response) and the excitation magnitude (force response) can be determined. The multiple solutions of the resonance amplitude that satisfy (16) either at different frequencies (Fig. 4) or excitation amplitudes (Fig. 5) are calculated numerically and plotted using Matlab for an arbitrary nonlinear resonant circuit parameters, assuming weak nonlinearity. The goal of this section is to briefly discuss the behavior of the Duffing-type resonant circuits. This behavior is exploited in explaining the working principle of the proposed nonlinear-resonant-based WPT circuits. Therefore, the analytical details are not provided while referring to [34] for more details.

Fig. 4(a) shows the typical frequency response of a nonlinear duffing resonator. The peak of the resonator's frequency

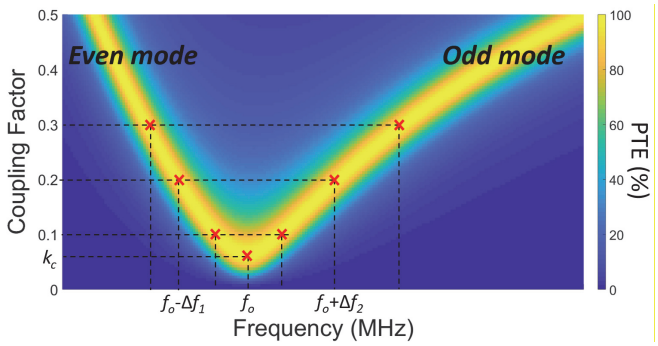

Fig. 6. PTE vs. frequency and coupling factor (k), showing the optimum operating frequency at different coupling factors.

response is tilted to the right or left, resulting in an increased bandwidth as compared to a linear resonator having a similar quality factor. The tilt direction of the amplitude-frequency response is dependent on ϵ. Positive ϵ causes the curve to tilt to the right (hardening systems), and a negative ϵ causes the curve to tilt to the left (softening systems). Since the nonlinear capacitor with a bell-shaped C-V curve shown in Fig. 3(a) has a positive nonlinear term, a_3, resonators utilizing such a nonlinear capacitors will have a frequency response that is tilted to the right (higher frequency). The tilting characteristic results in a three-root region as shown in Fig. 4(b). The region where there are three different solutions is called the bistable interval. The coexisting solutions forms the hysteresis where the trajectories initiated from different initial conditions can be attracted to different solutions. The stability of each solution can also be examined as illustrated in [34]. It can be proven that the medium solution points (represented by the dashed line) in this region are unstable, while the upper and lower points are stable and called equilibrium points [34]. As a result, the steady state solution of such a system converges to one of the two equilibrium solutions depending on the initial conditions. Moreover, the peak of the amplitude-frequency response can be predicted analytically [34]. In forced excitation of such resonators, like in WPT circuit described here, the source frequency is chosen to be at the same frequency of the highest resonance amplitude (denoted as f_o in Fig. 4(b)) allowing the maximum power to be delivered to the load.

The resonance response amplitude as a function of the excitation amplitude (V_s) at the desired source frequency is depicted in Fig. 5. As can be seen, when V_s increases quasi-statically from $V_s = 0$, the resonance amplitude increases gradually and moves on the lower equilibrium branch. When V_s reaches V_2, a jump-up in the response to the upper equilibrium branch is occurred. If V_s is decreased, a jump-down occurs at $V_s = V_1$. In particular, there are three coexisting solutions for $V_1 < V_s < V_2$ (the solid and dashed lines correspond to stable and unstable branches, respectively). The unique force-response characteristic of Duffing nonlinear resonators is very important in understanding the working principle of the proposed position-insensitive WPT circuits described in this paper. Generally, two resonators are coupled in a WPT system to transfer the power from the source to the load. As the

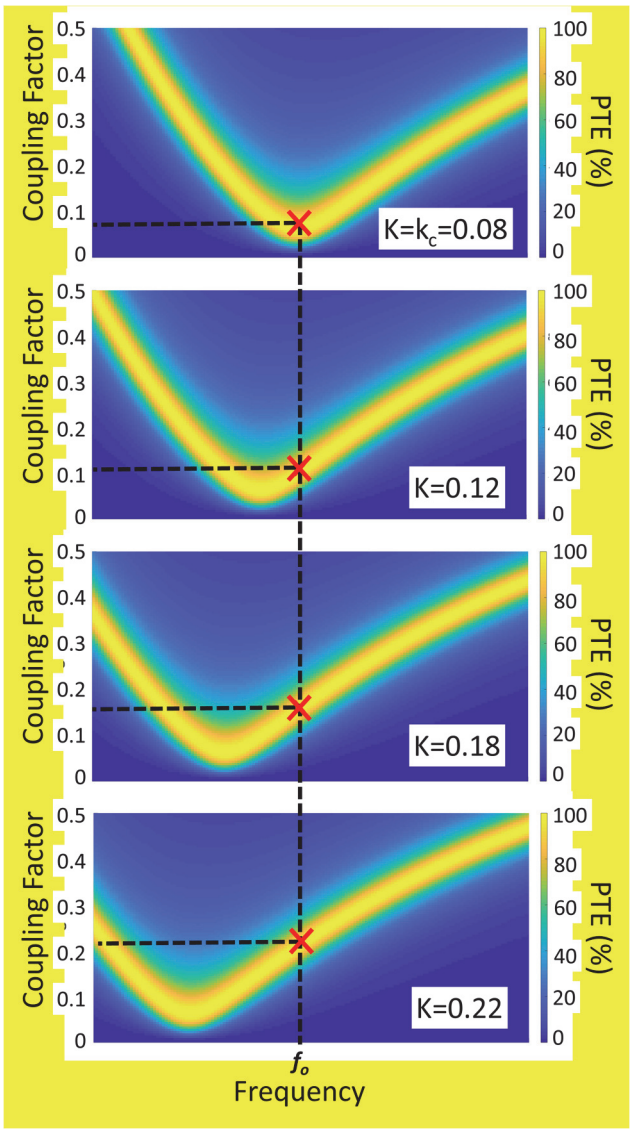

Fig. 7. Multiple plots of the PTE vs. frequency and coupling factor (k), associated with the adjusted resonance frequencies at different coupling factors.

coupling factor between the transmit and receive coils is varied, the amount of energy coupled to the receiver varies correspondingly. This can be modeled by an equivalent excitation source at the receiver side having a variable excitation amplitude ($V_s'(k)$) which is a function of the coupling between the transmitter and receiver. By employing a nonlinear resonator at the receiver side, the resonance amplitude can be maintained at its peak value regardless of the variation in the amplitude of the equivalent excitation source at the receiver due to the hysteretic response shown in Fig. 5. Hence, high PTE values can be maintained as the coupling factor varies without tuning the operating frequency.

III. PRINCIPLE OF OPERATION, ANALYSIS, AND DESIGN OF NONLINEAR RESONANT-BASED WPT CIRCUITS

The self-adaptive behavior of the nonlinear circuits described provide a novel solution to extend the transmission range of

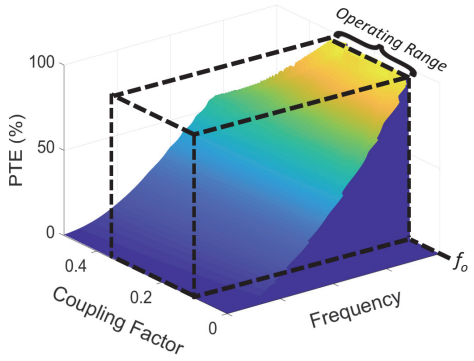

Fig. 8. PTE vs. operating frequency and coupling factor for the presented nonlinear resonant-based WPT circuits.

WPT systems over which the maximum PTE is maintained without varying the source frequency or employing any active feedback and control circuits. They provide a simple technique that allows a significant reduction in the sensitivity of WPT circuits to the variation of the coupling factor in real world operating conditions. In this section, the analysis, mathematical modeling, dynamical behavior, and the design methodology of the proposed nonlinear resonant-based WPT circuits are discussed.

Nonlinear resonant circuits are capable of adjusting their resonance frequencies based on the voltage amplitude across the nonlinear capacitors as can be seen from (13). Since the voltage amplitudes across the nonlinear capacitors in coupled nonlinear resonant circuits depend on the coupling factor, the resonance frequencies of the nonlinear resonators will be adjusted automatically based on the coupling factor. This self-adjustment characteristic is exploited to design the position-insensitive WPT circuit.

In this section, an arbitrary series-series WPT circuit, shown in Fig. 3, has been designed and simulated using the Advanced Design System (ADS) | Keysight simulator to generate the results shown in Fig. 6, 7, and 8. The scale of the frequency axis is normalized to the natural resonance frequency of the resonators, f_o, to generalize the discussion. The same simulation results and performance can be obtained for all different WPT circuit topologies at any operating frequency or power level based on the WPT application.

A. Principle of Operation

In order to visualize the operation of the proposed nonlinear resonant-based WPT circuit, the 3D plot of the PTE versus the frequency and the coupling factor (k), shown in Fig. 2, is plotted in 2D as shown in Fig. 6 (represented by the V-shaped curves). This figure shows the behavior of a conventional WPT circuit designed to operate at a critical coupling factor (k_c) operating at an arbitrary operating frequency, f_o. The principle of operation of conventional frequency tracking approach that relies on adjusting the operating frequency at each coupling factor is also shown in Fig. 6. The operating frequency is adjusted to track the optimum frequency (either odd or even modes) within the over-coupled region in order to maintain the maximum power transfer efficiency as the coupling factor varies.

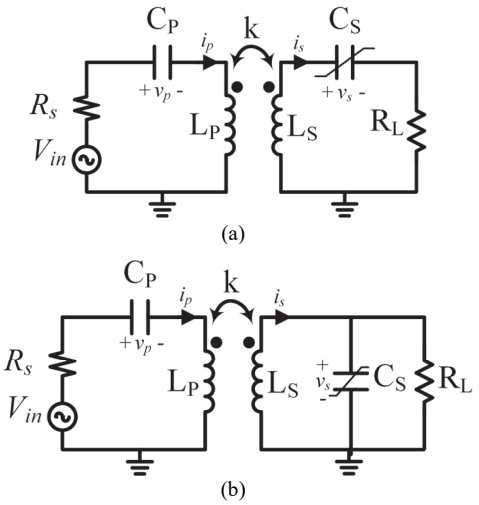

Fig. 9. Circuit schematics of the nonlinear resonant-based WPT (a) Series-Series topology, and (b) Series-Parallel topology.

On the contrary, the nonlinear resonant WPT circuits presented in this paper allow the circuit to maintain both the maximum power transfer and transfer efficiency at a fixed operating frequency as the coupling factor between the transmitter and the receiver is varied. The principle of operation for the position-insensitive WPT circuit is shown in Fig. 7. Multiple snapshots for shifted versions of the original V-shaped curve (shown in Fig. 6) at different coupling factors are plotted to demonstrate the operation of the nonlinear WPT circuits. The nonlinear WPT circuit's operation is visualized by sliding the position of the original V-shaped curve to lower or higher frequencies at each coupling factor such that a solution for maximum PTE exists at the same operating frequency. This can be achieved by tuning the values of the capacitors at each coupling factor.

This is achieved by utilizing a nonlinear resonant circuit which is capable of adjusting its resonance frequency automatically at each coupling factor since the voltage level across the nonlinear capacitor is a function of the coupling factor. A capacitor with a bell-shaped nonlinearity is utilized in this example, resulting in shifting the V-shaped curves to lower frequencies. Therefore, the WPT circuit effectively "tracks" the odd mode frequency response of the original linear WPT circuit. This self-adaptation mechanism is general as both the even and odd modes can be tracked based on the type of the device nonlinearity. Furthermore, PTE of the nonlinear resonant-based WPT circuit is simulated versus the frequency and coupling factor as shown in Fig. 8. The linear capacitors in the conventional WPT circuit are replaced with anti-series connected varactors to demonstrate the performance of the proposed nonlinear-resonant-based WPT circuit. As can be seen, the frequency splitting phenomena due to non-optimal matching is suppressed. At the desired operating frequency (f_o), the simulated WPT system provides a constant PTE over a wide range of coupling factors, as represented by the region inside dashed box.

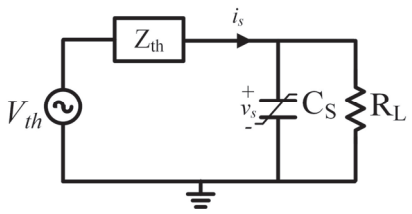

Fig. 10. The equivalent single nonlinear resonator at the receiver side of the series-parallel topology.

The enhancement of the nonlinear resonance WPT circuit's tolerance to coupling factor variation can also be understood by representing the nonlinear resonator's operation as a negative feedback. When the distance between the two coils is reduced, the coupling factor increases and the voltages across the nonlinear capacitors decreases due to the non-optimal matching. Therefore, the equivalent average capacitance (C_{eff}) increases. According to (13), the resonance frequency, ω_0, decreases which results in shifting of the V-shaped curve (Fig. 7) to a lower frequency allowing the maximum efficiency point to be tracked at the same desired frequency.

B. System Description and State-Space Modeling

The circuit schematics for series-series (SS) and series-parallel (SP) topologies of a resonant-based WPT circuit are shown in Fig. 9(a) and Fig. 9(b), respectively. The circuits' parameters are designed in order to provide resonant periodic waveforms of state variables namely, inductors' currents and capacitors' voltages. Application of the Kirchhoff's voltage law to the SS circuit topology shown in Fig. 9(a) results in:

$$i_p R_s + v_p + L_p\, di_p/dt - M\, di_s/dt = v_{in} \tag{19}$$

$$i_s R_l + v_s + L_s\, di_s/dt - M\, di_p/dt = 0 \tag{20}$$

where i_p, i_s, v_s and v_p are the state variables of the resonant-based WPT circuit that stand for the inductor currents and the capacitors' voltages in the primary and secondary sides, respectively. L_p, L_s, C_p, and C_s are respectively the inductances and capacitances in the primary and secondary sides. R_s and R_l are the source and load resistances, respectively.

Thus, the system state equations which describe the instantaneous nonlinear dynamics can be obtained from (19), (20), and using the time domain voltage-current relationship for capacitors [36]. The state equations are given by:

$$\dot{v_p} = i_p/C_p \tag{21}$$

$$\dot{v_s} = i_s/C_s \tag{22}$$

$$\dot{i_p} = \left[L_s v_{in} - L_s v_p - M v_s - L_s R_s i_p - M R_l i_s\right]/\Delta \tag{23}$$

$$\dot{i_s} = \left[M v_{in} - M v_p - L_p v_s - M R_s i_p - L_p R_l i_s\right]/\Delta \tag{24}$$

where $\Delta = L_s L_P - M^2 = L_s L_P(1-k^2)$.

Similarly, the system state equations for SP topology can be expressed by:

$$\dot{v_p} = i_p/C_p \tag{25}$$

$$\dot{v_s} = i_s/C_s - v_s/C_s R_l \tag{26}$$

$$\dot{i_p} = \left[L_s v_{in} - L_s v_p - M v_s - L_s R_s i_p\right]/\Delta \tag{27}$$

$$\dot{i_s} = \left[M v_{in} - M v_p - L_p v_s - M R_s i_p\right]/\Delta \tag{28}$$

Both topologies can be expressed by an equation of the form $\dot{x}(t) = Ax(t) + u(t)$, where

$$x(t) = \left[v_p(t) \quad v_s(t) \quad i_p(t) \quad i_s(t)\right]^T \tag{29}$$

$$u(t) = [0 \quad 0 \quad L_S/\Delta \quad M/\Delta]^T . v_{in}(t) \tag{30}$$

$$A_{SS} = \begin{bmatrix} 0 & 0 & \frac{1}{C_p} & 0 \\ 0 & 0 & 0 & \frac{1}{C_s} \\ \frac{-L_s}{\Delta} & \frac{-M}{\Delta} & \frac{-L_s R_s}{\Delta} & \frac{-MR_l}{\Delta} \\ \frac{-M}{\Delta} & \frac{-L_p}{\Delta} & \frac{-MR_s}{\Delta} & \frac{-L_p R_l}{\Delta} \end{bmatrix} \tag{31}$$

$$A_{SP} = \begin{bmatrix} 0 & 0 & \frac{1}{C_p} & 0 \\ 0 & \frac{-1}{C_s R_l} & 0 & \frac{1}{C_s} \\ \frac{-L_s}{\Delta} & \frac{-M}{\Delta} & \frac{-L_s R_s}{\Delta} & 0 \\ \frac{-M}{\Delta} & \frac{-L_p}{\Delta} & \frac{-MR_s}{\Delta} & 0 \end{bmatrix} \tag{32}$$

The parameters of the matrix A for both SS and SP circuit topologies are functions of the primary and secondary components. Thus, the equations that describe the dependence of the nonlinear devices (either capacitive or inductive) on the system's states can be evaluated and substituted into the matrix A. The solution for $x(t)$ starting from an initial time instant and an initial state, x_0, can be expressed by using Euler's method to approximate the differential equations by discrete difference equations is given:

$$x(t+1) = (I + A.\Delta t)x(t) + u(t).\Delta t \tag{33}$$

where I is the identity matrix. In this paper, we study the effect of employing a nonlinear capacitor at the secondary side, $C_s(v_s)$, upon the circuit's performance of the series-parallel topology.

C. Synthesizing the C-V Relationship for the Secondary Nonlinear Capacitor

Since the nonlinear device is employed at the receiver side, an equivalent single nonlinear resonant circuit is realized at the receiver circuit in order to simplify the determination of the required nonlinearity while reducing the simulation time. The primary and secondary inductors are assumed to be equal, $L_p = L_s = L$. The linear series resonant circuit at the primary side is reflected to the receiver side after the secondary inductor as shown in Fig. 10 by calculating the Thevenin Equivalent circuit as follows:

$$V_{th} = \frac{-\omega^2 C_p L k}{(1-\omega^2 L C_p) + j\omega C_p R_s} \times V_{in} \tag{34}$$

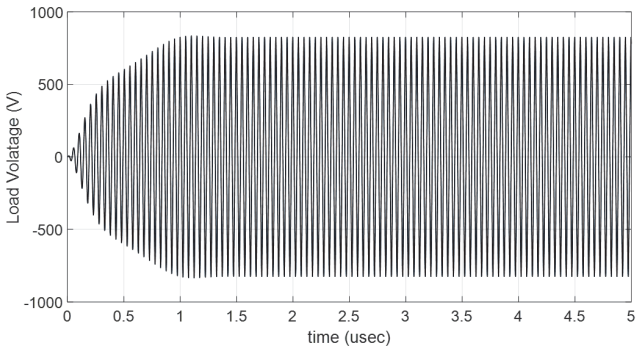

Fig. 11. Simulated transient response of the voltage across a 5kΩ load resistance in the proposed nonlinear resonant-based WPT circuit at k=0.22. (The source available power is 60 W)

$$Z_{th} = \frac{-\omega^2 C_p L R_s + j\omega L\left(1-\omega^2 L C_p\left(1-k^2\right)\right)}{\left(1-\omega^2 L C_p\right)+j\omega C_p R_s} \tag{35}$$

Therefore, the real and imaginary parts of the Thevenin impedance can be expressed as:

$$Re\{Z_{th}\} = \frac{\omega^4 C_p^2 M^2 R_s}{\left(1-\omega^2 L C_p\right)^2+\omega^2 C_p^2 R_s^2} \tag{36}$$

$$Im\{Z_{th}\} = \omega L - \frac{\omega^3 C_p M^2\left(\omega^2 L C_p-1\right)}{\left(1-\omega^2 L C_p\right)^2+\omega^2 C_p^2 R_s^2} \tag{37}$$

The resonance frequency of the primary resonator is designed to be the same as operating frequency, $\omega_{o,p} = 1/\sqrt{LC_p} = \omega$. Accordingly, (34), (36), and (37) expressions can be reduced to:

$$V_{th}(\omega = \omega_o) = jkQ_{l1}V_{in} \tag{38}$$

$$Re\{Z_{th}(\omega = \omega_o)\} = \frac{\omega^2 k^2 L^2}{R_s} = Q_{lp}^2 k^2 R_s \tag{39}$$

$$Im\{Z_{th}(\omega = \omega_o)\} = \omega L \tag{40}$$

where $Q_{lp} = \omega L_p/R_s$ is the loaded quality factor of the primary resonator. It can be seen that V_{th} is function of the coupling factor. The state-space modeling of the single equivalent resonant circuit hence can be evaluated as:

$$\begin{bmatrix}\dot{v}_s\\ \dot{i}_s\end{bmatrix} = \begin{bmatrix}-1/C_s(v_s)R_l & 1/C_s(v_s)\\ -1/L & -Q_{lp}^2 k^2 R_s/L\end{bmatrix}\begin{bmatrix}v_s\\ i_s\end{bmatrix} + \frac{k}{L}\begin{bmatrix}0\\ Q_{lp}\end{bmatrix} v_{in} \tag{41}$$

Finally, the power delivered to the load and the corresponding overall PTE can be calculated as

$$P_{out} = V_s^2/2R_l \tag{42}$$

$$PTE = P_{out}/P_{av} = \frac{V_s^2/2R_l}{V_{in}^2/8R_s} \tag{43}$$

Using (41) and (43), the C-V relationship of the nonlinear capacitor ($C_s(v_s)$) can be synthesized such that high PTE is maintained across the required coupling factor range. A search algorithm is utilized to optimize the design parameters for different types of nonlinear capacitors. For example, the anti-series varactor diodes' C-V equation can be given by:

$$C = \frac{C_{j0}}{\left(1-\frac{V_{j1}}{V_{bi}}\right)^{\gamma}} \,||\, \frac{C_{j0}}{\left(1-\frac{V_{j2}}{V_{bi}}\right)^{\gamma}} \tag{44}$$

where C_{j0} is the zero-bias junction capacitance, V_{j1} is the junction voltage across first diode, V_{j2} is the junction voltage across the second diode where $v_{j1} + v_{j2} = v_s$, V_{bi} is the built-in potential, and γ is the grading coefficient. Thus, the design parameters are C_{j0}, V_j and γ. Alternatively, the nonlinear capacitor can be expressed by the following polynomial form:

$$C = C_0 + C_1 V + C_2 V^2 + C_3 V^3 \tag{45}$$

where C_0, C_1, C_2, and C_3 are the optimization parameters. Using the aforementioned system analysis, the time domain transient and steady-state waveforms and the FFT spectra of the output power delivered to the load can be numerically simulated using Matlab. Fig. 11(a) shows the simulated transient response of the nonlinear WPT circuit, using the aforementioned analysis. A very small amount of overshooting is observed in the transient response which does not affect the operation of the circuit.

Based on the analysis provided in this section, the design methodology can be summarized in three steps. The first step is to design a linear WPT circuit to fulfil the required WPT circuit specifications in terms of operating frequency, targeted power level, desired transmission range, and load value. The second step is to determine the optimum nonlinearity required to maintain the PTE over the desired range of coupling factor values. This is achieved through optimization tools in circuit simulators. Finally, the third step is to synthesize the required nonlinearity using through different combination of the available commercial nonlinear devices that can provide the proper nonlinearity while handling the targeted power levels. In the following section, the implementation and measurement results for the position-insensitive WPT circuit prototype is discussed in details".

IV. Nonlinear WPT Circuit Implementation and Experimental Results

As a proof of concept, a WPT circuit employing a nonlinear resonator in the receiver side has been designed and implemented. The WPT primary circuit is capable of transmitting 60 W to a resistive load of 2.5 kΩ in the secondary circuit at 2.25 MHz. Initially, a 60 W conventional linear WPT reference circuit has been designed. The value of the load resistance was chosen based on the targeted critical coupling factor ($k_c = 0.14$) corresponding to a 25 cm transmission distance between the two coils used in this setup. Recalling that, $k_c = 1/\sqrt{Q_p Q_s}$ [4], where $Q_p = \omega_o L_p/R_{source}$ is the loaded quality factor of the primary series resonant circuit and $Q_s = R_{load}/\omega_o L_s$ is the loaded quality factor of the secondary parallel resonance circuit. Knowing the values of $k_c, Q_p, Q_s, L_p, L_s, R_{source}, and\ \omega_o$, the load value has been determined to be 2.5 kΩ. A real RF load resistor was used during the measurements while the light bulb with equivalent

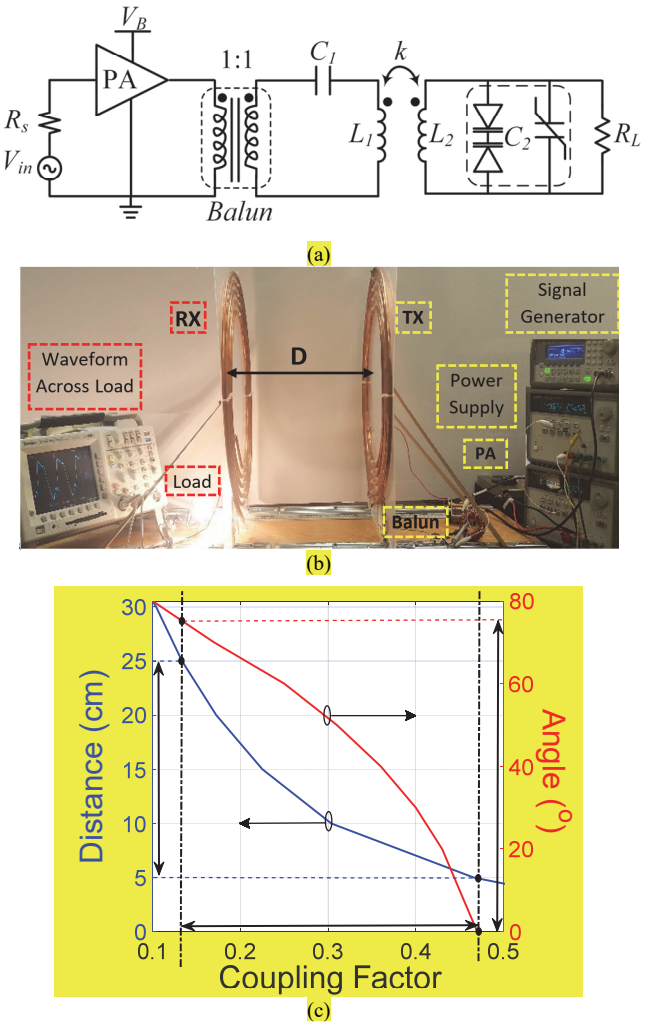

Fig. 12. Implemented series-parallel topology of the position-insensitive WPT circuit: (a) circuit schematic, (b) experiment setup, and (c) measured coupling factor between the transmit and receive coils versus the transmission distance and the angular misalignment.

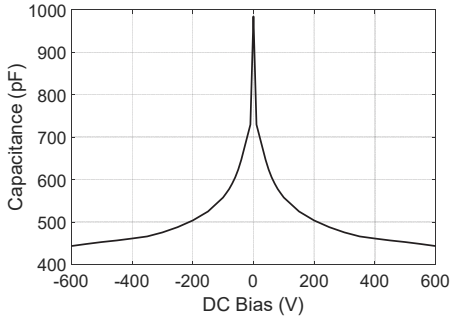

Fig. 13. Measured C-V response of the optimized combination of the nonlinear capacitors.

TABLE I
COMPONENT SPECIFICATIONS FOR THE IMPLEMENTED WPT CIRCUIT

Component	Specification
Transmit and Receive Coils	
Inductance	15 μH
Outer Diameter	40 cm
Inner Diameter	25 cm
Pitch	1 cm
Number of turns	5
Primary Capacitor	350 pF
Secondary Capacitor	Shunt combination of: 1. Anti-series connection of SiC STPSC20H12-Y 1.2kV Schottky diodes 2. Series & parallel combinations of high-voltage nonlinear X7R ceramic capacitors (equivalent DC capacitance = 200 pF)
Load Resistor	2.5 kΩ

resistance, shown in Fig. 12(b), was used for the performance's demonstration purposes only [38]. While the load resistance value might seem very large, the proposed technique is generic and can be applied to design any WPT circuit with particular specifications including the load value. The circuit topology (i.e. the type of resonance, series or parallel) is decided based on the equivalent load impedance of the rechargeable battery.

The prototype was mounted on ball bearing sliders to allow for a smooth movement of the receiving coil with respect to the transmitting coil. It is noteworthy to point out that the circuit's power level and frequency can be scaled up and down to address the required specifications for different applications or to comply with a standard. In this experiment, series-parallel topology is utilized and the circuit schematic as well as the experiment setup employing a 2.5 kΩ load, are shown in Fig. 12(a) and 12(b), respectively. A signal generator is used to feed the transmitter's linear power amplifier (PA) and the output of the PA is then connected to the transmit circuit through a 1:1 balun. The available power from the power amplifier is 60 W (the maximum power level that PA can provide to a perfectly matched load at that frequency). A typical class-A RF power amplifier with an efficiency of ~30% is utilized in the experiment. The efficiency of the PA is not included in the reported PTE of the proposed WPT circuit. On the receiver side, the receive coil is connected in parallel with the passive nonlinear capacitor and the load resistor. The load resistor value is determined based on the loaded quality factor of the resonators required to satisfy the critical coupling factor. Both the transmit and receive coils have 5 turns with inner diameter of 25 cm, outer diameter of 40 cm, a pitch of 1 cm. Table I summarizes the component specifications for the implemented WPT circuit.

The measured coupling factor values as function of: (1) the transmission distance and (2) the angle between the transmit and receive coils at 20 cm transmission distance, are shown in Fig. 12(c). Based on [37], the coupling factor is proportional to $\cos(\alpha)$, where α is the angle between the normal vectors to the coils' planes. Afterwards, the design procedure discussed in Section III is followed to synthesize the required nonlinearity at the receiver side such that a high PTE is maintained within the operating range. The C-V curve of the optimized nonlinear device is measured and shown in Fig. 13. This nonlinearity is realized using a combination of an anti-series connected SiC STPSC20H12-Y 1.2kV Schottky diodes in shunt with a

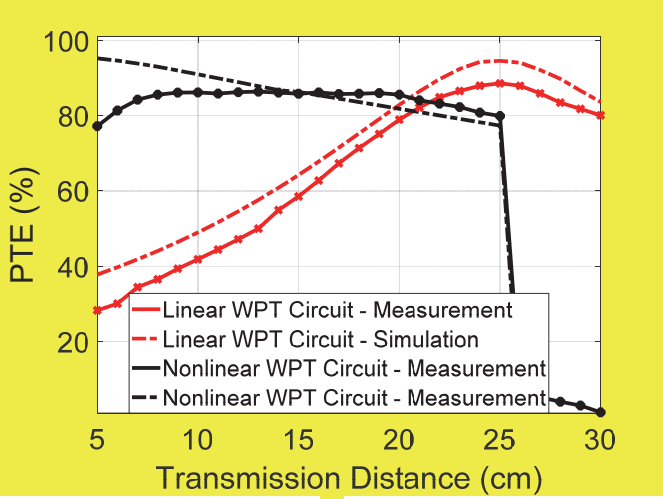

(a)

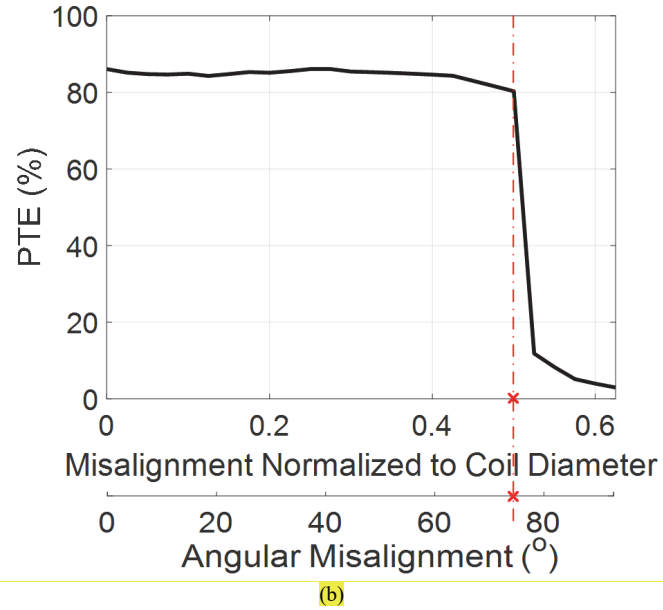

(b)

Fig. 14. Measured PTE versus (a) distance variation, and (b) lateral misalignment offset between the transmit and receive coils.

combination of several high-voltage, low-loss nonlinear ceramic capacitors of Class II (X7R) which exhibit strong voltage dependent capacitance behavior when driven with high voltage swings [39].

The output power delivered to a real 2.5 kΩ resistive load is measured as a function of the transmission distance (D) and lateral misalignment. The PTE is defined as the ratio of the load power to the PA output available power. Therefore, the impedance mismatch at the PA output port is taken into account when calculating PTE. However, the power efficiency of the PA itself is not included in the measured PTE values. The measured received power is approximately 51 W with max variation of 3 W over a distance variation from 5 cm to 25 cm. The simulation results (dashed lines) in comparison with the measurement results (solid lines) of the PTE versus transmission distance for both the nonlinear WPT circuit (black lines) and the corresponding linear WPT circuit, using the same experimental setup, (red lines) are shown in Fig. 14(a). The measured results show a good agreement with the simulation results especially at low coupling factor values. However, there is a slight discrepancy between them at high coupling factor values (transmission distance range between 5 cm and 10 cm). This is expected to be due to the discrepancy between the measured and modeled C-V curves of the nonlinear devices in addition to the inaccurate modeling of the circuit losses as a function of the temperature and the large signal across the nonlinear devices. These effects can be mitigated by careful optimization for the circuit setup in the simulation environment. More careful modeling optimization would result in a better agreement between the simulation and measurement results.

As depicted in Fig. 14(a), a maximum PTE of 86% in the conventional linear WPT circuit is measured at transfer distance of 25 cm (corresponding to the critical coupling factor for this setup) and decreases as distance varies in both directions (towards and away from the source). At the same time, not only the nonlinear WPT circuit achieves the same peak PTE of 86%, it maintains the high PTE over distance variation of $\Delta D = \pm 10$ measured from the center operating transfer distance ($D = 15\ cm$). Compared to a conventional WPT circuit using the same experimental setup, the high-efficient operating transmission range, defined with a PTE higher than 80%, extends by 200%, and the efficiency at the shortest transmission distance (5 cm) improves by about 2.6 times.

The proposed position-insensitive WPT circuit compensates for the effect of the coupling factor variation on the PTE within a specific range based on the circuit nonlinearity. The value of the coupling factor is highly dependent on the relative position between the transmit and receive coils in terms of the vertical transmission distance, lateral misalignment, and angular misalignment. Therefore, the tolerable range of coupling factor translates into an efficient 3D charging zone for a wireless charger where the high PTE and the targeted power level are maintained independent on the position and orientation of the device. In this paper, the implemented WPT circuit tolerates a variation in the coupling factor value between 0.14 and 0.47, as shown in Fig. 12(c).

Motivated by that, the robustness of the nonlinear WPT circuit as a function of the lateral and angular misalignments between the transmit and receive coils are tested. Fig 14(b) shows the measured PTE as a function the lateral misalignment, normalized to the diameter of the coil measured at the center operating distance ($D = 15\ cm$), and the angular misalignment in degrees measured at a transmission distance of 20 cm. The peak PTE is maintained when lateral misalignment is increased up to +/- 20 cm (±50% of the coil diameter). Moreover, the circuit maintains the same peak PTE when varying the angle between the transmit and receive coils up to $\pm 75^{o}$. The tolerable ranges of the lateral and angular misalignments map to the same coupling factor range that can be tolerated by the circuit's nonlinearity. Furthermore, both ranges are function of the transmission distance between the centers of the coils since it affects the overall value of the coupling factor as well.

The jump-down that appears in the PTE curve at the critical coupling distance is imposed by the hysteresis characteristic of the nonlinear resonators. It can be proved that there is no valid

solution for high PTE to exist at the operating frequency within the under-coupled region. For nonlinear WPT circuits, the critical coupling distance defines the upper boundary of the efficient transmission range which is designed based on the required system specifications.

The robust nonlinear resonant-based WPT circuit introduced in this paper promises the 3-dimentional positioning freedom in WPT systems allowing efficient wireless power transfer, without requiring precision positioning or alignment over the charging pad. The presented technique is applicable to a broad range of operating conditions including operating distances, frequencies, or power ranges. Therefore, WPT circuits based on nonlinear resonance can have a significant impact on the performance of WPT systems operating in real world environments.

V. Conclusion

This paper presents a novel technique using nonlinear passive devices to design position insensitive WPT circuits which maintain their performance independent of the coupling factor between the transmit and receive coils. The position insensitive WPT circuit introduced here is entirely passive, simple and highly reliable as it does not require any active feedback control circuits, source frequency tuning, tunable matching networks, and controllers. A 60 W WPT circuit prototype designed based on such technique is implemented and its performance is measured. The circuit exhibits a near-constant efficiency of approximately 80% operating at 2.25 MHz over: (1) distance variation, ΔD, of up to +/- 10 cm from the center operating transfer distance ($D_o = 15\ cm$), (2) lateral misalignment of up to ±50% of the coils' diameter at the center operating distance, and (3) angular misalignment of up to ±75°.

References

[1] X.Z. Wei, Z. Wang, H. Dai, "A critical Review of Wireless Power Transfer via Strong Coupled Magnetic Resonances", *Energies 2014*, vol. 7, pp. 4316-4341, July 2014.

[2] K. Wu, D. Choudhury and H. Matsumoto, "Wireless Power Transmission, Technology, and Applications [Scanning the Issue]," in *Proceedings of the IEEE*, vol. 101, no. 6, pp. 1271-1275, June 2013.

[3] S. Y. R. Hui, W. Zhong and C. K. Lee, "A Critical Review of Recent Progress in Mid-Range Wireless Power Transfer," in *IEEE Transactions on Power Electronics*, vol. 29, no. 9, pp. 4500-4511, Sept. 2014.

[4] A. P. Sample, D. T. Meyer and J. R. Smith, "Analysis, Experimental Results, and Range Adaptation of Magnetically Coupled Resonators for Wireless Power Transfer," in *IEEE Transactions on Industrial Electronics*, vol. 58, no. 2, pp. 544-554, Feb. 2011.

[5] P. S. Riehl et al., "Wireless Power Systems for Mobile Devices Supporting Inductive and Resonant Operating Modes," in *IEEE Transactions on Microwave Theory and Techniques*, vol. 63, no. 3, pp. 780-790, March 2015.

[6] S. Lee and R. D. Lorenz, "Development and Validation of Model for 95%-Efficiency 220-W Wireless Power Transfer Over a 30-cm Air Gap," in *IEEE Transactions on Industry Applications*, vol. 47, no. 6, pp. 2495-2504, Nov.-Dec. 2011.

[7] J. Dai and D. C. Ludois, "Capacitive Power Transfer Through a Conformal Bumper for Electric Vehicle Charging," in *IEEE Journal of Emerging and Selected Topics in Power Electronics*, vol. 4, no. 3, pp. 1015-1025, Sept. 2016.

[8] C. Liu, A. P. Hu and N. K. C. Nair, "Modelling and analysis of a capacitively coupled contactless power transfer system," in *IET Power Electronics*, vol. 4, no. 7, pp. 808-815, Aug. 2011.

[9] R. Dias Fernandes, J. N. Matos and N. Borges Carvalho, "Resonant Electrical Coupling: Circuit Model and First Experimental Results," in *IEEE Transactions on Microwave Theory and Techniques*, vol. 63, no. 9, pp. 2983-2990, Sept. 2015.

[10] S. Li and C. C. Mi, "Wireless Power Transfer for Electric Vehicle Applications," in *IEEE Journal of Emerging and Selected Topics in Power Electronics*, vol. 3, no. 1, pp. 4-17, March 2015.

[11] Kurs, A., Karalis, A., Moffatt, R., Joannopoulos, J. D., Fisher, P., & Soljačić, M. (2007). Wireless power transfer via strongly coupled magnetic resonances. *Science*, *317*(5834), 83-86.

[12] S. I. Babic and C. Akyel, "Calculating Mutual Inductance Between Circular Coils With Inclined Axes in Air," in *IEEE Transactions on Magnetics*, vol. 44, no. 7, pp. 1743-1750, July 2008.

[13] R. Huang, B. Zhang, D. Qiu and Y. Zhang, "Frequency Splitting Phenomena of Magnetic Resonant Coupling Wireless Power Transfer," in IEEE Transactions on Magnetics, vol. 50, no. 11, pp. 1-4, Nov. 2014, Art no. 8600204.

[14] J. D. Heebl, E. M. Thomas, R. P. Penno and A. Grbic, "Comprehensive Analysis and Measurement of Frequency-Tuned and Impedance-Tuned Wireless Non-Radiative Power-Transfer Systems," in *IEEE Antennas and Propagation Magazine*, vol. 56, no. 5, pp. 131-148, Oct. 2014.

[15] J. Park, Y. Tak, Y. Kim, Y. Kim, and S. Nam, "Investigation of adaptive matching methods for near-field wireless power transfer," in *IEEE Trans. Antennas Propag.*, vol. 59, no. 5, pp. 1769–1773, May 2011.

[16] Wenzhen Fu, Bo Zhang and Dongyuan Qiu, "Study on frequency-tracking wireless power transfer system by resonant coupling," *2009 IEEE 6th International Power Electronics and Motion Control Conference*, Wuhan, 2009, pp. 2658-2663.

[17] B.-J. Jang, S. Lee, and H. Yoon, "HF-Band Wireless Power Transfer System: Concept, Issues, and Design," *Progress In Electromagnetics Research*, Vol. 124, 211-231, 2012.

[18] T. C. Beh, M. Kato, T. Imura, S. Oh and Y. Hori, "Automated Impedance Matching System for Robust Wireless Power Transfer via Magnetic Resonance Coupling," in *IEEE Transactions on Industrial Electronics*, vol. 60, no. 9, pp. 3689-3698, Sept. 2013.

[19] Benjamin H. Waters and Joshua R. Smith, "Adaptive impedance matching for magnetically coupled resonators." *PIERS Proceedings*. 2012.

[20] J. Lee, Y. Lim, W. Yang and S. Lim, "Wireless Power Transfer System Adaptive to Change in Coil Separation," in *IEEE Transactions on Antennas and Propagation*, vol. 62, no. 2, pp. 889-897, Feb. 2014.

[21] Y. Lim, H. Tang, S. Lim and J. Park, "An Adaptive Impedance-Matching Network Based on a Novel Capacitor Matrix for Wireless Power Transfer," in *IEEE Transactions on Power Electronics*, vol. 29, no. 8, pp. 4403-4413, Aug. 2014.

[22] J. Kim and J. Jeong, "Range-Adaptive Wireless Power Transfer Using Multiloop and Tunable Matching Techniques," in *IEEE Transactions on Industrial Electronics*, vol. 62, no. 10, pp. 6233-6241, Oct. 2015.

[23] G. Lee, B. H. Waters, Y. G. Shin, J. R. Smith and W. S. Park, "A Reconfigurable Resonant Coil for Range Adaptation Wireless Power Transfer," in *IEEE Transactions on Microwave Theory and Techniques,* vol. 64, no. 2, pp. 624-632, Feb. 2016.

[24] T. P. Duong and J. Lee, "Experimental Results of High-Efficiency Resonant Coupling Wireless Power Transfer Using a Variable Coupling Method," in *IEEE Microwave and Wireless Components Letters*, vol. 21, no. 8, pp. 442-444, Aug. 2011.

[25] Y. Lyu et al., "A Method of Using Nonidentical Resonant Coils for Frequency Splitting Elimination in Wireless Power Transfer," in *IEEE Transactions on Power Electronics*, vol. 30, no. 11, pp. 6097-6107, Nov. 2015.

[26] W. Lee, W. Son, K. Oh and J. Yu, "Contactless Energy Transfer Systems Using Antiparallel Resonant Loops," in *IEEE Transactions on Industrial Electronics*, vol. 60, no. 1, pp. 350-359, Jan. 2013.

[27] S. Assawaworrarit, X. Yu, S. Fan." Robust wireless power transfer using a nonlinear parity-time symmetric circuit" Nature 546 (2017), 387-390.

[28] X. Y. Zhang, C. D. Xue and J. K. Lin, "Distance-Insensitive Wireless Power Transfer Using Mixed Electric and Magnetic Coupling for Frequency Splitting Suppression," in *IEEE Transactions on Microwave Theory and Techniques*, vol. 65, no. 11, pp. 4307-4316, Nov. 2017.

[29] X. Wang and A. Mortazawi, "Duffing resonator circuits for performance enhancement of wireless power harvesters," *2015 IEEE*

MTT-S International Microwave Symposium, Phoenix, AZ, 2015, pp. 1-4.
[30] X. Wang, "High Efficiency and High Sensitivity Wireless Power Transfer and Wireless Power Harvesting Systems," Ph.D. dissertation, Radiation Lab., Univ. of Michigan, Ann Arbor, 2016.
[31] A. Mortazawi, and X. Wang. "Nonlinear Resonance Circuit for Wireless Power Transmission and Wireless Power Harvesting." U.S Patent publication 20160336810, application date: May 12, 2015.
[32] X. Wang and A. Mortazawi, "Bandwidth Enhancement of RF Resonators Using Duffing Nonlinear Resonance for Wireless Power Applications," in *IEEE Transactions on Microwave Theory and Techniques*, vol. 64, no. 11, pp. 3695-3702, Nov. 2016.
[33] X. Wang, O. Abdelatty and A. Mortazawi, "A novel coupling factor independent highly efficient resonant based wireless power transfer," *2017 47th European Microwave Conference (EuMC)*, Nuremberg, 2017, pp. 200-203.
[34] Kovacic, I., & Brennan, M. J. (2011). *The Duffing equation: Nonlinear oscillators and their behaviour*. Wiley.com.
[35] Clary Jr William, T. "Nonlinear resonant circuit devices." U.S. Patent 2,838,687, June 10, 1958.
[36] E. Bou-Balust, A. El Aroudi, P. Fisher and E. Alarcon, "Unveiling nonlinear dynamics in resonant inductively coupled wireless power transfer," *2014 IEEE International Symposium on Circuits and Systems (ISCAS)*, Melbourne VIC, 2014, pp. 2612-2615.
[37] E. R. Joy, A. Dalal and P. Kumar, "Accurate Computation of Mutual Inductance of Two Air Core Square Coils with Lateral and Angular Misalignments in a Flat Planar Surface," in *IEEE Transactions on Magnetics*, vol. 50, no. 1, pp. 1-9, Jan. 2014, Art no. 7000209
[38] https://www.youtube.com/watch?v=palcyBurQLs&feature=youtu.be
[39] H. P. Jeon, Y. K. Choi, S. W. Kim, D. K. Choi, "Simulation and Characterization for the Non-Linearity of Multilayer Ceramic Capacitors with New Equivalent Circuits under Ac-Field", *Solid State Phenomena, Vols. 124-126, pp. 827-830, Jun. 2007*

Omar Abdelatty (S'15) was born in Cairo, Egypt. He received the B.Sc. and M.Sc. degrees from Cairo University, Egypt, in 2012 and 2015, respectively, and is currently working toward the Ph.D. degree in electrical engineering at University of Michigan, Ann Arbor, USA.

From 2012 to 2015, he was with Cairo Circuits and Systems Laboratory (CCSL), Cairo University. His current research interests include nonlinear circuits' analysis and design, wireless power transfer systems, and low power RF and mm-wave circuit design.

Xiaoyu Wang (S'13-M'16) received the B.S. degree in electrical engineering from Tsinghua University, Beijing, China, in 2011, and the Ph.D. degree from The University of Michigan at Ann Arbor in 2016.

He is currently with Qualcomm Technologies Inc. His research interests include RFIC, on-chip electromagnetics, and wireless power transfer/harvesting systems.

Amir Mortazawi (M'90-SM'05-F'06) received the Ph.D. degree in electrical engineering from The University of Texas at Austin, Austin, USA, in 1990.

He is currently a Professor of electrical engineering with The University of Michigan, Ann Arbor, MI, USA. His current research interests include millimeter-wave phased arrays, power amplifiers, power-combining techniques, wireless power transmission and harvesting, and frequency-agile microwave circuits. Dr. Mortazawi was a member of the IEEE Microwave Theory and Techniques Society (IEEE MTT-S) Administrative Committee for three terms. He is the Vice-Chair of the IEEE MTT-13 Committee on Microwave Control Materials and Devices. He was the Editor-in-Chief of the IEEE TRANSACTIONS ON MICROWAVE THEORY AND TECHNIQUES from 2006 to 2010. He served as an Associate Editor of the IEEE TRANSACTIONS ON MICROWAVE THEORY AND TECHNIQUES in 2005, an Associate Editor of the IEEE TRANSACTIONS ON ANTENNAS AND PROPAGATION from 1998 to 2001, and the Guest Editor of the 1995 IEEE TRANSACTIONS ON MICROWAVE THEORY AND TECHNIQUES' "Special Issue on the IEEE MTT-S Microwave Symposium."